

An Embroidered Two-Dimensional Chipless Strain Sensor For Wireless Structural Deformation Monitoring

Arnaud Vena, *Member, IEEE*, Karoliina Koski, *Student Member, IEEE*, Elham Moradi, *Student Member, IEEE*, Abdul Ali Babar, *Student Member, IEEE*, Lauri Sydänheimo, *Member, IEEE*, Leena Ukkonen, *Member, IEEE*, and Manos M. Tentzeris, *Fellow, IEEE*

Abstract—A wireless chipless sensor for structural deformation monitoring is proposed. The sensor is based on two resonant scatterers sewn on stretchable fabrics with conductive threads. The combination of the two scatterers allows for the detection of the strain in a 2-D plane. The backscattered response, as a function of frequency, is detected with the help of frequency-stepped continuous wave radar technique. The radar performs the detection by scanning the two orthogonal polarizations. It operates in the ISM band at 2.45 GHz. The proposed processing method achieves the 2-D extraction of the strain and the tensile force with the electromagnetic response of the sensor. Simulation and measurement results validate this new concept.

Index Terms—Chipless sensor, deformation, fabrics, sewn, stretchable, strain, stress, conformal sensor, smart skin, SHM structures.

I. INTRODUCTION

WIRELESS sensors are becoming ubiquitous in many applications since they can often be distributed over large surfaces in a seamless way for a lower cost than wired solutions. Besides, over the last decade passive radio frequency identification (RFID) sensing technology [1]–[5] has been under investigation as a potential solution to overcome the major issue of remote sensors, that is, the maintenance of their battery. A passive RFID sensor gets energy from the electromagnetic (EM) field of the remote reading system. This means that it doesn't require any battery to operate. However, conventional RFID sensors in their simplest form suffer from some issues due to their fabrication process variability, even when assembled with chips and antennas of similar types. These issues tend to lower the detection accuracy of RFID sensors. To alleviate these issues while decreasing

simultaneously the unit cost of the sensors, the chipless sensor technology [6]–[16] proposes an interesting alternative. At the expense of a poor coding capacity compared to a conventional RFID sensor, chipless sensors provide accuracy, repeatability and mechanical robustness for a cost that can be dramatically decreased. The uncertainties in manufacturing for a chipless sensor are only due to the antenna realization, whereas the antenna connection to the chip, and the chip impedance, are additional uncertainty sources in conventional RFID technology. A chipless tag [17]–[23] doesn't embed any integrated circuit (IC). It can be seen as an arrangement of one or several antennas with a short as load. In conventional RFID's, the reader has to detect, for a single frequency, the difference of the tag's radar cross section (RCS) between the two impedance states of the chip connected with the antenna. On the contrary, a chipless tag always reflects the same RCS response per frequency over a narrow or wide frequency range of interrogation. In other words, it can be considered as a static radar target for a given transmitting incident angle. Commonly, the detection can be performed with a frequency-stepped continuous-wave radar (FSCW) [24], a frequency-modulated continuous-wave radar (FMCW) [25], or an impulse radio ultra-wide band (IR-UWB) radar [26]. The analysis of the RCS as a function of the frequency is one way to encode an identifier (ID) [19]–[22], or to sense a physical parameter [11], as depicted in Fig. 1.

A previous work showed that it was possible to realize chipless tags and sense the strain in one direction with sewn tags on fabrics [27]. This new work focuses on a technique to monitor and extract the 2-dimensional (2-D) strain/stress over the surface of an object. We present thereafter, the design of a low cost chipless sensor, based on two scatterers sewn on stretchable fabrics. The conductive threads used for this purpose, provide reliability to mechanical stress, resistance to water, as well as wearability and wrappability properties [28]–[31]. A computer-aided sewing machine can be used to realize an antenna pattern with a typical accuracy of 1 mm as shown in [29]–[31]. The targeted applications concern mainly object realized with fabrics such as cord links. However, sewn sensors can also be bonded on object surfaces for structural health monitoring of buildings as shown in Fig. 1. Detecting a strain or a crack with chip-based sensors [4]–[5] and chipless sensors [8]; [12] has been recently studied and shows the growing interest for this field of research. The main advantage

Manuscript received April 22, 2013; revised June 20, 2013; accepted June 26, 2013. Date of publication July 9, 2013; date of current version October 4, 2013. This work was supported in part by the Finnish Funding Agency for Technology and Innovation, and Academy of Finland and Centennial Foundation of Finnish Technology Industries. The associate editor coordinating the review of this paper and approving it for publication was Dr. M. R. Yuce.

A. Vena, K. Koski, E. Moradi, A. Ali Babar, L. Sydänheimo, and L. Ukkonen are with the Tampere University of Technology, Tampere 33720, Finland (e-mail: arnaud.vena@tut.fi; karoliina.koski@tut.fi; elham.moradi@tut.fi; abdul.babar@tut.fi; lauri.sydanheimo@tut.fi; leena.ukkonen@tut.fi).

M. M. Tentzeris is with Georgia Tech, Atlanta, GA 30332-250 USA (e-mail: etentze@ece.gatech.edu).

Color versions of one or more of the figures in this paper are available online at <http://ieeexplore.ieee.org>.

Digital Object Identifier 10.1109/JSEN.2013.2272493

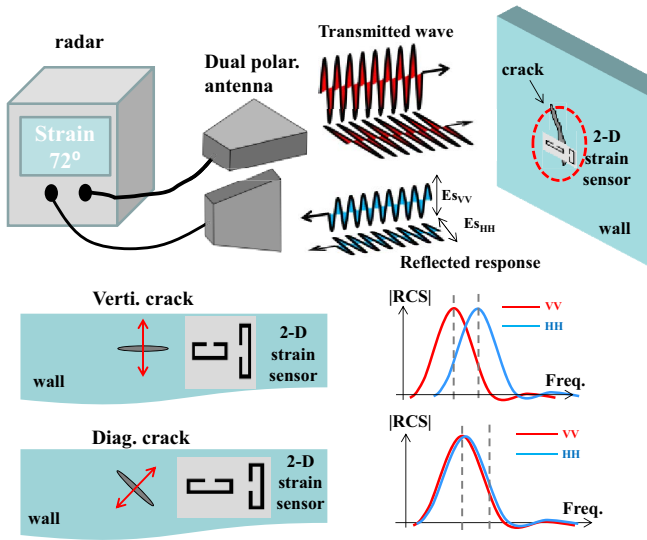


Fig. 1. Principle of a wireless monitoring system for crack detection. Chipless sensor is applied on a wall to detect cracks and deformation in 2-D.

of this new concept is the possibility to sense a 2-D strain with a low-cost design realized on a flexible and highly stretchable substrate. Fabric has been used because it is a resistant material, low-cost and largely stretchable. In addition, it can fit any shape. Further, it has been demonstrated in [33], that fabric embedding electro-thread can be advantageously used for crack or strain detection for civil infrastructure monitoring. The main reason is that large surfaces can be covered with a low cost sensitive “smart skin” film.

Section II presents the design of a sewn strain sensor operating in dual-polarization. Then in section III, we propose a measurement setup to monitor the variation of the RCS as a function of the strain and the tensile force, applied to the sensor in 2-D. In section IV we present a novel technique to extract strain values based on RCS measurements. A discussion about the achieved performance as well as about practical implementation issues will precede the conclusion.

II. DESIGN OF A SEWN 2-DIMENSIONAL SENSOR

To make a strain sensor, we first require a stretchable material with repeatable properties after several uses. For this purpose, fabrics are well suited. For the realization of the sensor we use a polyester-based stretchable fabric. They are composed of durable and stretchable threads. A permittivity value of 1.4 with a $\tan \delta$ of 0.022 at 2.45 GHz has been measured with an Agilent dielectric probe kit 85070E. Over the last few years, it has become possible to sew conductive circuits with the help of electro-threads for seamless integration with clothes or monitored structure surfaces (e.g. supporting beams). Thus, a wireless chipless sensor, that is effectively just a passive electric circuit, can be realized based on the aforementioned technique.

A. Design of a Dual 90° Rotated SRR Based Sensor

To allow for the detection of a strain in 2-D, we utilized two polarizations orthogonal to each other. Each one is

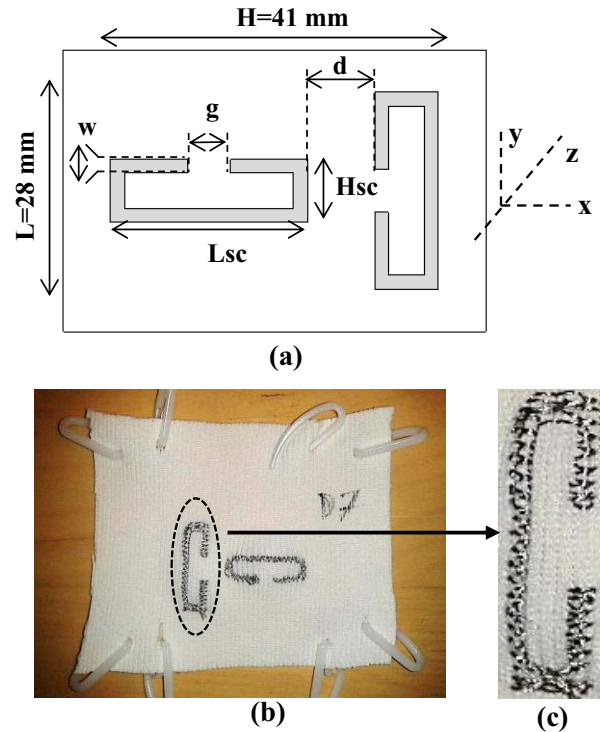


Fig. 2. (a) 2-D sensor design based on orthogonal arranged rectangular SRR. (b) View of the sewn sensor on polyester-based stretchable fabric. (c) Magnification of the sewn scatterer. The dimensions are $w=2$ mm, $g=6$ mm, $H_{sc}=9$ mm, $L_{sc}=28$ mm, $d=10$ mm.

providing information about the strain component to its respective axis/direction. The RCS variation detected in the vertical polarization may inform about a strain along the vertical axis, whereas the horizontal polarization is useful to detect a strain in the horizontal axis. To be able to separate the strain in 2-D, the RCS variation of the utilized sensor has to be significantly different as a function of polarization. This means that a sensor that provides the same amplitude or frequency variation in both polarizations when subject to a strain in one axis cannot be used.

The design presented in Fig. 2(a) and (b) is composed of two identical scatterers 90° rotated, one with respect to each other. The scatterer shape is a rectangular split ring resonator (SRR). The use of a rectangle, instead of a square SRR enhances the strain sensitivity along one direction. This particular shape is chosen in order to limit the structural mode that may interfere with the resonant mode that carries the strain information for a given axis. For comparison, in a configuration with two closed-loop 90° rotated scatterers, there exists a strong coupling between the orthogonal loops, whereas it is not the case with SRR scatterers. Further, a resonant mode correlated with the total length of the open loop appears with a SRR, whereas for a closed loop, the first resonant mode is correlated with its demi-length. This effectively reduces the size of the loop by two to achieve the same resonant frequency. Figure 3 showing the surface current distribution in horizontal polarization at the resonance of 4.9 GHz, for the two closed-loop 90° rotated scatterers, confirms their strong coupling. These simulation results have been obtained with CST Microwave Studio using a plane wave as for excitation.

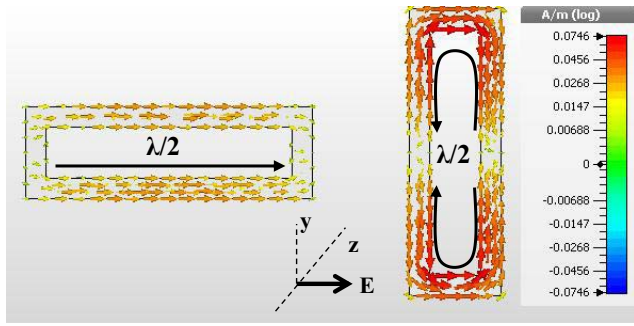


Fig. 3. Surface current distribution at 4.9 GHz in horizontal polarization for two closed loop 90° rotated scatterers.

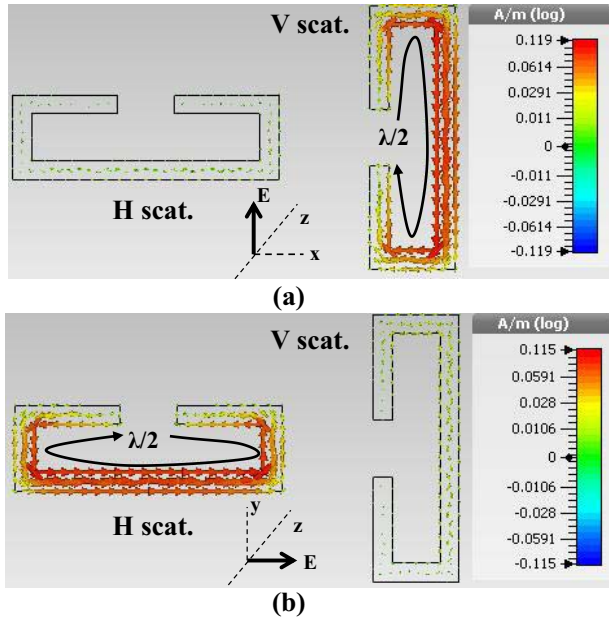


Fig. 4. Surface current distribution at 2.45 GHz for the 90° rotated SRR based sensor (a) in vertical polarization, and (b) in horizontal polarization.

Besides, Fig. 4(a) and (b) show the surface current paths at 2.45 GHz, for the sensor-based rectangular SRR, in vertical and horizontal polarization, respectively. For the vertical polarization, we notice a standing wave mode linked to the electric length of the scatterer denoted “V scat.,” meanwhile almost no current is flowing into the “H. scat.” For the horizontal polarization (see Fig 4 (b)), the standing wave mode is linked to the scatterer denoted “H scat.,” whereas the “V. scat.” element is not excited. This confirms that there is a very low coupling between two 90° rotated SRR’s for any given polarization. Figure 5 shows the RCS of a single SRR optimized to operate at 2.45 GHz for different polarizations (VV and HH). Due to the different lengths of the horizontal and the vertical parts of the scatterer, its RCS shows a resonant peak at various frequencies depending of polarization. A RCS difference close to 25 dB between the two polarizations at 2.45 GHz is noted. This difference explains why the rotated SRR are not coupled at 2.45 GHz for a given polarization.

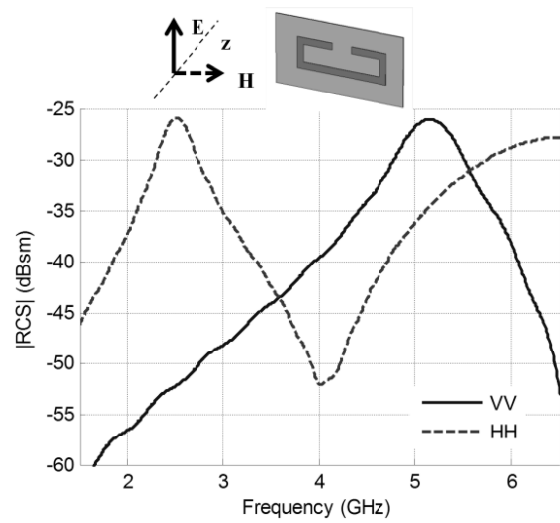


Fig. 5. Simulated |RCS| response of a single rectangular SRR for the two orthogonal polarizations. The dimensions are given in Fig. 2.

Achieving the desired radiating performances requires the optimization of the scatterers’s dimensions. A very important design parameter for all sewn implementations is the relatively high conduction losses of the metallic threads and the minimum gap separation to avoid unwanted short. A high-quality factor cannot be achieved simply by decreasing the size of the gap or the width of the strips as it is the case when using low loss metals. On the contrary, when dealing with high loss conductors, their cross section (mainly the width) has to be increased, to reduce the linear resistance of the strips. Besides, to achieve a good RCS, which is directly correlated with the maximum detection range, the size of the loop has to be large enough. Finally, the design parameters used for this study have been obtained with the help of an optimization under CST Microwave studio. The fixed parameter was the strip width ($w = 2$ mm) to guarantee conductors having a low resistance. We noticed that a larger value is not recommended, because this increases the structural mode. The length ($L_{sc} = 28$ mm), the height ($H_{sc} = 9$ mm) and the gap ($g = 6$ mm) were free to be modified. The goals of the optimization were a RCS above -30 dBsm at 2.45 GHz with the best quality factor. The separation distance value ($d = 10$ mm) between the two scatterers is a tradeoff between coupling effect and sensor size.

Figures 6(a) and (b) show the RCS variation in the two polarizations when the sensor is submitted to a strain along the vertical axis and the horizontal axis respectively. We notice that the peak is modified, both in amplitude and in resonant frequency for the two polarizations. However, in Fig. 6(a) the vertical polarization response is much more affected by the applied strain along the vertical axis compared to the horizontal polarization response. Inversely, in Fig. 6(b) the opposite behavior can be obtained when applying a strain along the horizontal axis. It is proven in section IV that this difference of RCS variation is enough to separate the strain in 2-D.

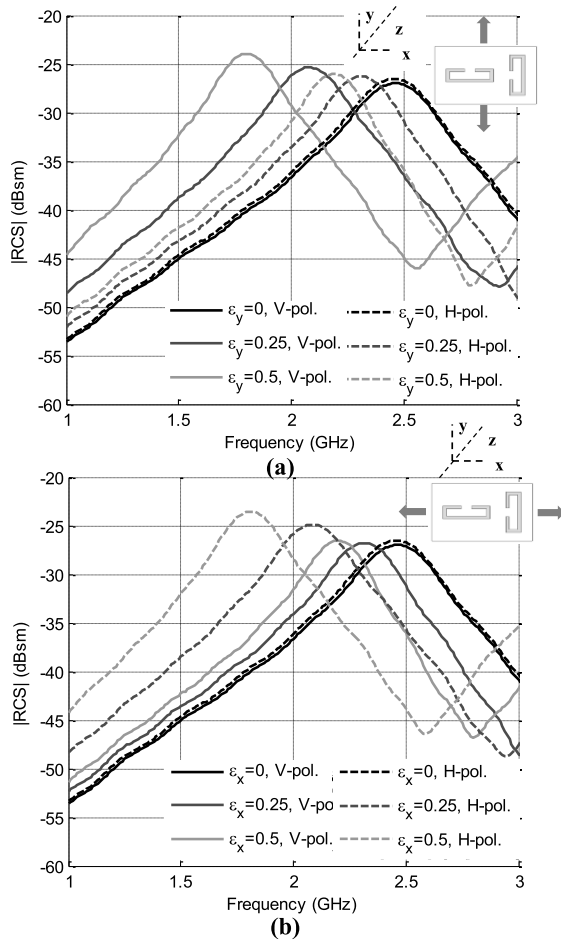


Fig. 6. Simulated $|RCS|$ for both polarizations (a) for a strain ε_y applied along the vertical axis and (b) for a strain ε_x applied along the horizontal axis. The dimensions are given in Fig. 2.

B. Implementation of the Sewn Sensor

Shieldex 110f34 dtex 2-ply HC [32] electro-thread is used to sew the scatterers due to the fact that this type of thread is compatible with the use of a computer-aided sewing machine. Thus, for the realization of the sensor shown in Fig. 2(a) and (b), we used a Husqvarna Viking machine featuring a resolution of 1 mm. This limitation has been taken into account for the design of the tag that operates around 2.45 GHz. The electro-thread is composed of 34 filaments plated with silver. It has a DC linear resistivity of $500 \Omega\text{m} \pm 100 \Omega\text{m}$. However, a conductive strip of few millimeters of width is composed of tens of threads. At low frequencies, the resistivity of the strip can be estimated by dividing the resistivity of one thread by the number of threads that compose the strip. In wireless and radio frequencies, this simple approximation cannot be used, but a recent study [30] shows that a sewn strip can be approximated by an effective bulk conductor having the same dimensions as for the sewn strip. For the one used in this work (see Fig. 2(c)), we found that a conductivity value close to $3 \times 10^3 \text{ S/m}$ allows for the good agreement of simulations and measurements. The parameters to consider for the enhancement of the conductivity value are the density of stitches per surface unit, and the orientation of the threads.

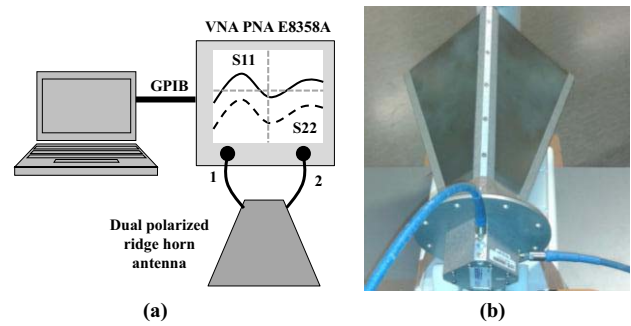


Fig. 7. (a) Measurement test bench principle. (b) View of the dual polarized antenna.

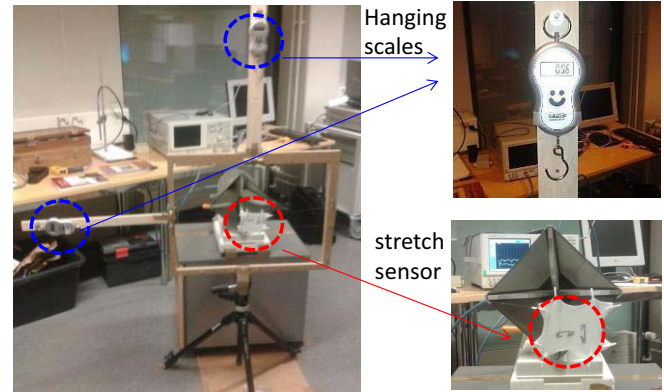


Fig. 8. View of the strain and stress test-bench for 2-D tensile force detection and strain detection. The strain is measured with a ruler, whereas the tensile force is measured with hanging scales.

Indeed, to get the best radiating performance, the threads have to be aligned along the surface currents. The design presented Fig. 2(b) has been sewn with 386 stitches. The tension of the thread during the sewing has been tuned to a minimum value in order to increase the flexibility of the sensor when stretched. We observed that the used fabric is more easily stretchable along the horizontal axis. Thus, different results will be obtained when regarding the two strain axes.

III. MEASUREMENT SETUP AND RESULTS

A frequency-domain measurement setup is used to wirelessly monitor, the RCS variation of the strain sensor. For this purpose, we implement a mono-static frequency-stepped continuous wave (FSCW) radar as depicted in Fig 7(a) and (b). A two-port vector network analyzer (VNA) Agilent PNA E8358A is connected to a dual-polarization wide-band antenna ETS Lindgren 3164-04 having a gain of 9 dBi around 2.45 GHz. The ports 1 and 2 of the VNA are connected with the vertical and the horizontal polarization inputs of the antenna, respectively. The output power is 0 dBm for both ports. Thus, the measured scattering parameters S11 and S22 contain the EM responses from the background and the tag, in vertical polarization and in horizontal polarization, respectively. A calibration described in [22] allows for the separation of the tag response from the background response. A picture of the measurement setup can be seen in Fig. 8(a). As one can see, the tag is placed on a mechanical stretching

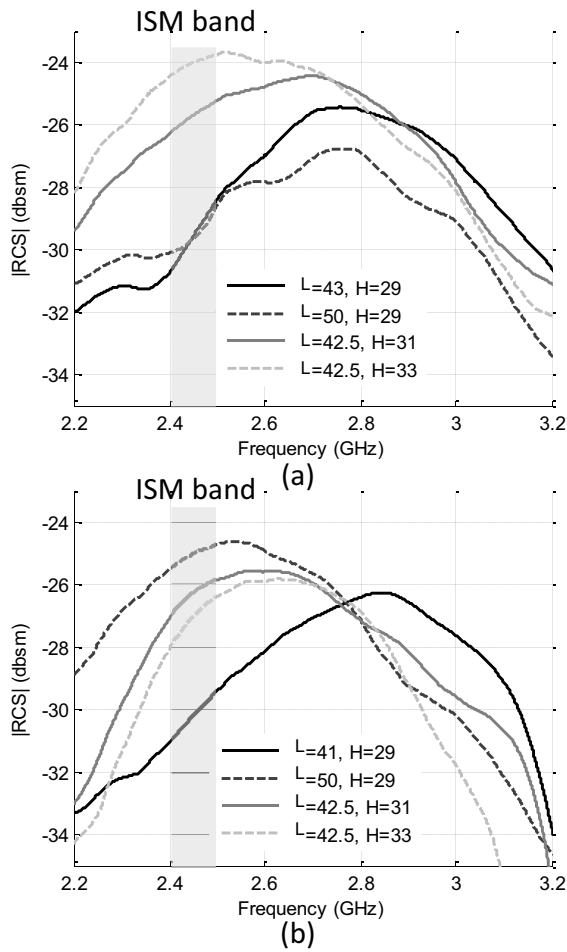


Fig. 9. |RCS| measurement results for various randomly distributed strain configurations (a) in vertical polarization and (b) in horizontal polarization. The measured dimensions L and H (see Fig. 2 (a)) are given in mm for each configuration.

test bench at 20 cm away from the horn aperture. The test bench is composed of a wooden frame, on which two hanging scales are placed to measure a tensile force in 2-D. The tensile force is applied to the stretchable sensor via fishing wires. This force can be varied by changing the tension applied to the wires. The hanging scale has an accuracy of 0.5 N for a range from 0 to 400 N. The tag is placed in the middle of the wooden frame, so that no metallic part is interfering during the measurement, as shown in Fig. 8.

Figures 9(a) and (b) show the measured EM response for several tensile forces applied to the sensor in vertical and horizontal polarization, respectively. We chose the tensile force configurations to get a good measurement coverage within full-range values in 2-D. Both the maximum RCS, and the frequency of the peak value are affected, as expected. It should be noted that a variation of the tensile force in vertical axis induces a strong resonant frequency variation in vertical polarization, and a weak variation in horizontal polarization. This behavior is reciprocal for a variation of the tensile force along the horizontal axis.

We carried out repetitive measurements to study separately the effect of each stretching axis on the EM response of the corresponding polarization. For this purpose, a cycle of

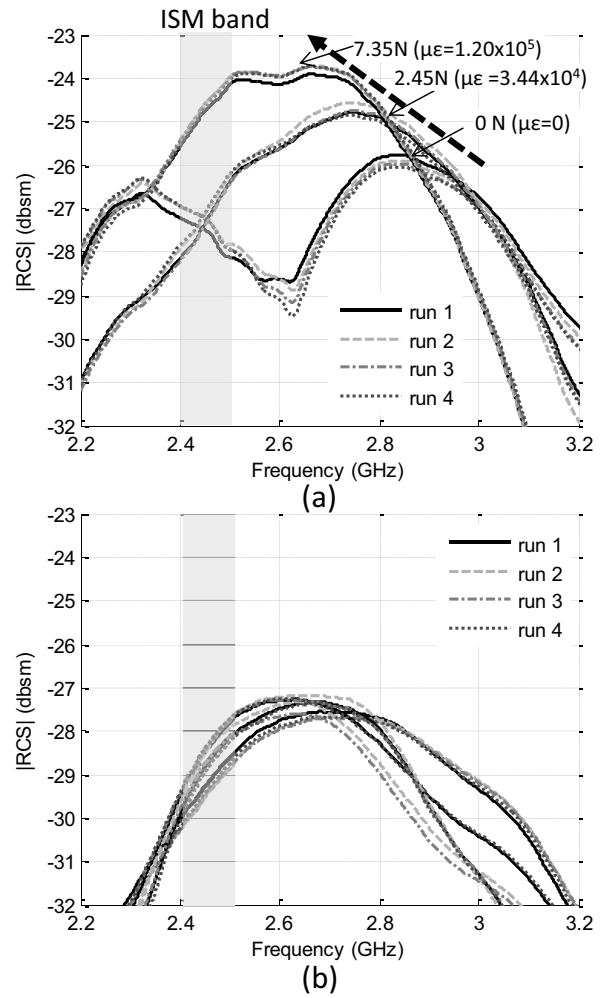


Fig. 10. |RCS| measurement results for repetitive strain configurations along the vertical axis, (a) in vertical polarization and (b) in horizontal polarization. The measures are repeated four times for each strain configuration, that are, for 0 N ($\mu\epsilon = 0$), 2.45 N ($\mu\epsilon = 3.44 \times 10^4$) and 7.35 N ($\mu\epsilon = 1.2 \times 10^5$).

three different tensile forces has been measured and repeated four times, making a total of 12 measurements for each axis. Figures 10(a) and (b) show the RCS of the sensor in vertical and horizontal polarization, respectively, when the force is applied in the vertical axis only. Similarly, Fig. 11(a) and (b) show the RCS responses when the force is applied along the horizontal axis. The RCS curves measured for each given tensile force show a common shape. This confirms a very close correlation between the measurements of the four cycles. It should be noted that, around 2.45 GHz, a large RCS variation is observed for the polarization aligned with the pulling axis, whereas, for the orthogonal polarization, no significant difference is noted. A difference of 1 dB concerning the peak value (from 26 dB to 27 dB) can be noted for the orthogonal polarization between Fig. 10(a) and Fig. 11(a). This is due to an unwanted small movement of the sensor position when subject to a tensile force. In the following part, we will discuss a method to detect the strain in both axes based on single or multi-linear approximations of the relationship between the RCS responses and the applied force values.

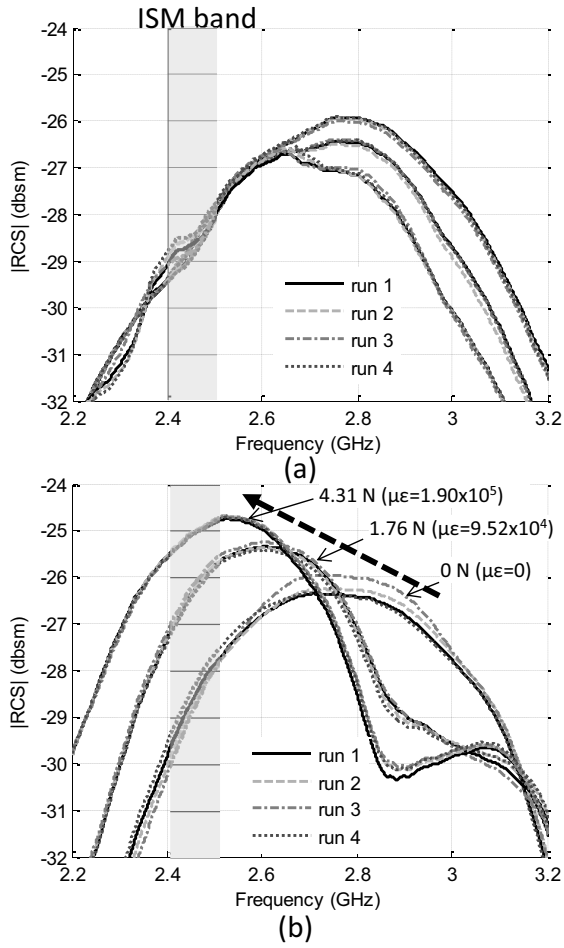


Fig. 11. $|RCS|$ measurement results for repetitive strain configurations along the horizontal axis, (a) in polarization VV and (b) in polarization HH. The measures are repeated four times for each strain configuration, that are, for 0 N ($\mu\epsilon = 0$), 1.76 N ($\mu\epsilon = 9.52 \times 10^4$) and 4.31 N ($\mu\epsilon = 1.9 \times 10^5$).

IV. EXTRACTION OF A 2-D STRAIN

A. Extraction Based on a Single Linear Approximation

Figure 12(a) shows the extracted relationship between, the tensile force applied in vertical axis, and the measured RCS measured at 2.45 GHz for the vertical polarization. Figure 12(b) shows the same relationship for the horizontal tensile force, and the EM response in horizontal polarization. Figures 13(a) and (b) show the extracted relationship between the strain (defined as micro-strains ($\mu\epsilon$)) and the RCS at 2.45 GHz, along the vertical axis and the horizontal axis, respectively. The definition of a micro-strain is provided in (1) with ΔL , the difference length due to the strain, and L_0 the initial length without strain.

$$\mu\epsilon = \frac{\Delta L}{L_0} \cdot 10^6 \quad (1)$$

A decoding technique based on the use of 1st order polynomial model for each axis is possible. However, it features significant tensile force errors close to 2 N in vertical axis, and 1.85 N in horizontal axis. The maximum strain errors are for the vertical and the horizontal axis $2.58 \times 10^4 \mu\epsilon$ and $8.3 \times 10^4 \mu\epsilon$, respectively. In many cases, this accuracy is not

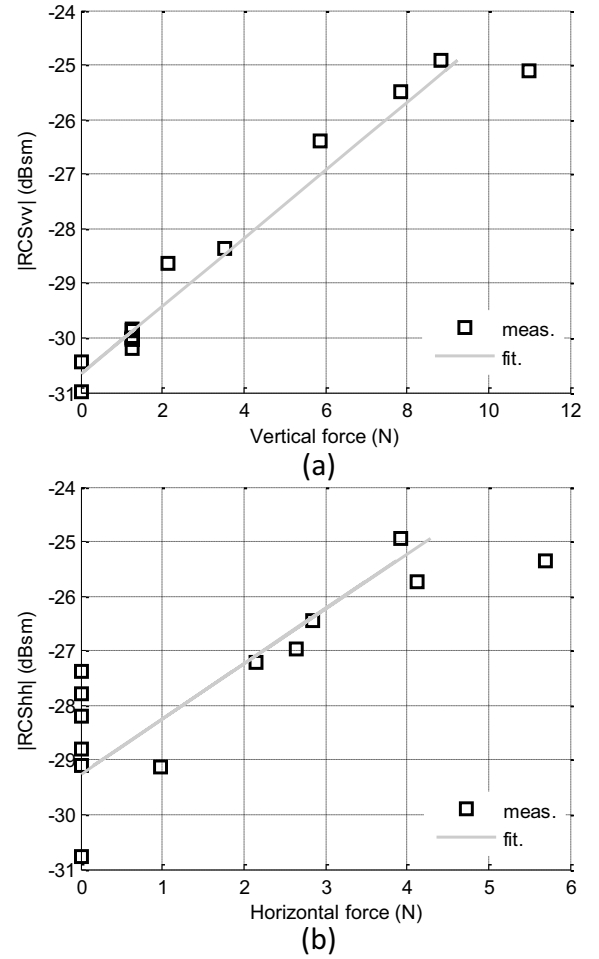


Fig. 12. Extracted relationship between $|RCS|$ at 2.45 GHz and tensile force (a) along the vertical axis and (b) along the horizontal axis. For each axis the fitted curve is based on a single linear regression model with 13 measurements.

sufficient for practical applications. To further improve it, we have to define a more complete model that takes into account the cross relations between the two polarizations. Moreover, the aforementioned technique uses only the RCS level at one frequency point. The technique suffers from poor reliability because the measured RCS is strongly affected by the background noise. This decreases the accuracy of the single linear regression model.

B. Extraction Based on a Combination of Orthogonal Polarization RCS With a Two-Step Processing

We found that a technique based on the shape of RCS curves measured in two polarizations, for a given configuration, provides more accurate results. Further, this increases robustness because even in presence of additional noise, the shape roughly remains the same after filtering. Figure 14 shows some of the measured EM responses in the ISM band from 2.4 GHz to 2.5 GHz. One can notice that they can be approximated by a polynomial of the first order. To find the coefficients of these polynomials, a linear regression is applied based on the numerous frequency points measured in the band from 2.4 to 2.5 GHz. For this experiment a frequency resolution

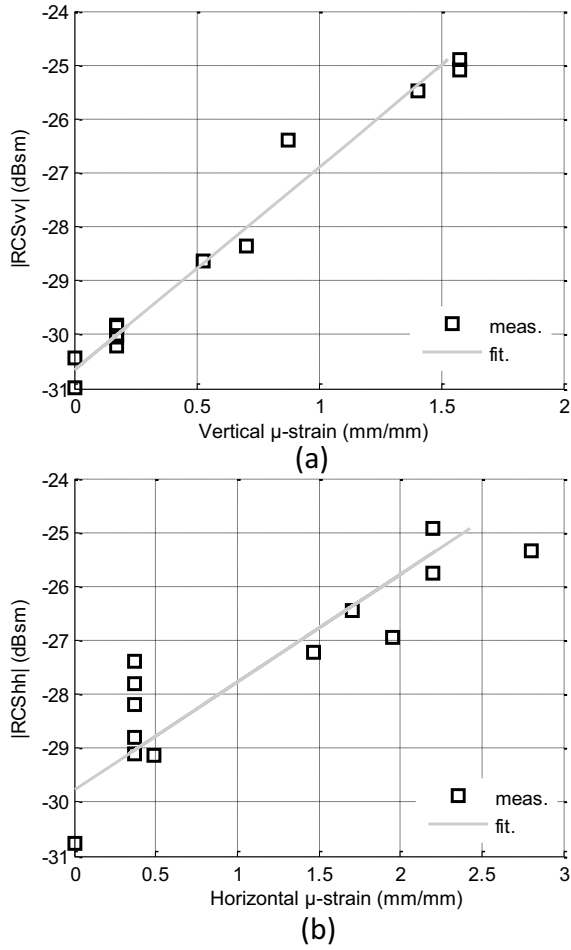


Fig. 13. Extracted relationship between $|RCS|$ at 2.45 GHz and tensile force (a) along the vertical axis and (b) along the horizontal axis. For each axis the fitted curve is based on a single linear regression model with 13 measurements.

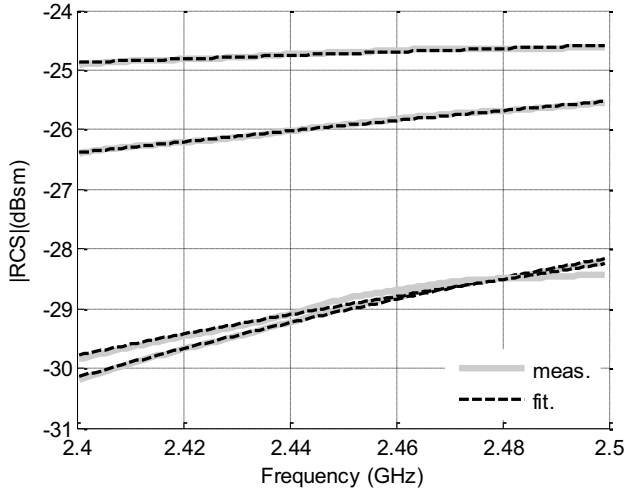


Fig. 14. Zoom of the measured $|RCS|$ for several strain configuration within the ISM band in vertical polarization. A polynomial approximation of the 1st order is used to extract the polynomials coefficients a and b according to equation (2).

of 1 MHz has been used, so that, 100 frequency points are measured. It is noteworthy that, the more number of points,

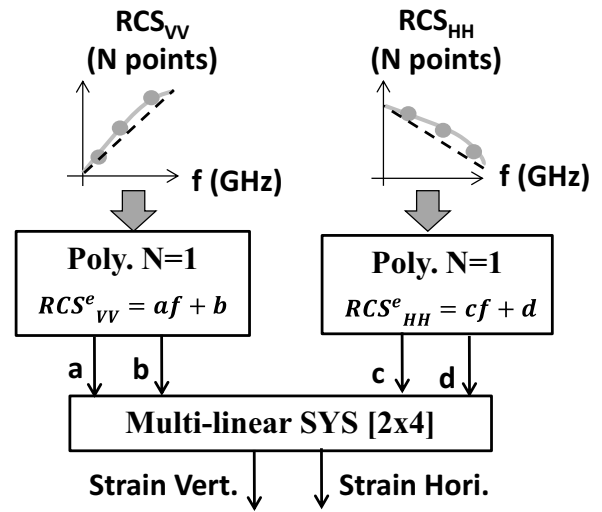


Fig. 15. Principle of the 2-D strain extraction technique based on a two-step processing.

the higher is the accuracy of the approximation, even though it takes more time. Moreover, with numerous frequency points, the rejection of the added random noise to the RCS response is better. As shown in Fig 10 and 11, the resonant peak is not centered in the ISM band from 2.4 and 2.5 GHz, but we found that a more accurate model is obtained in this case because RCS magnitude differences between various strains are more significant. Further, because resonant peaks in both polarizations are located above the ISM band, we can precisely model RCS variation in this frequency span by 1st order polynomial curves. The model presented in Fig. 15 has been utilized for the extraction of a relationship between the measured EM responses in the two polarizations and the 2-D strain as follows:

- The first step is to calculate the polynomial coefficients of the EM response from 2.4 GHz to 2.5 GHz in both polarizations.
- Then the coefficients become the inputs of a multi linear regression system which gives in return, the strain in 2-D.

Equations (2) and (3) give the approximated polynomials at the 1st order, of the EM responses in vertical and horizontal polarization, respectively. The coefficients a , b , c and d are extracted from the measured RCS responses for frequencies f between 2.4 GHz and 2.5 GHz. Equation (4) provides the tensile force \underline{F} values in 2-D as a function of the polynomial coefficients of the estimated RCS responses $\underline{RCS}_{coeff}^e$. In this study, the multi-linear model \underline{L} is extracted based on ten RCS measurements for random tensile forces in 2-D. The test-bench allows varying the tensile force from 0 N to 11 N in the horizontal axis and from 0 N to 5.5 N in the vertical axis. The corresponding strains can vary from $0 \mu\epsilon$ to $1.6 \times 10^5 \mu\epsilon$ and from $0 \mu\epsilon$ to $2.8 \times 10^5 \mu\epsilon$, in the vertical and horizontal axis, respectively. Equation (4) can be rewritten as (5), in matrix form. The terms L_{ij} define the Linear model L , and the model outputs F_v and F_h are the tensile forces or strains in 2-D.

$$RCS_v^e = a \cdot f + b \quad (2)$$

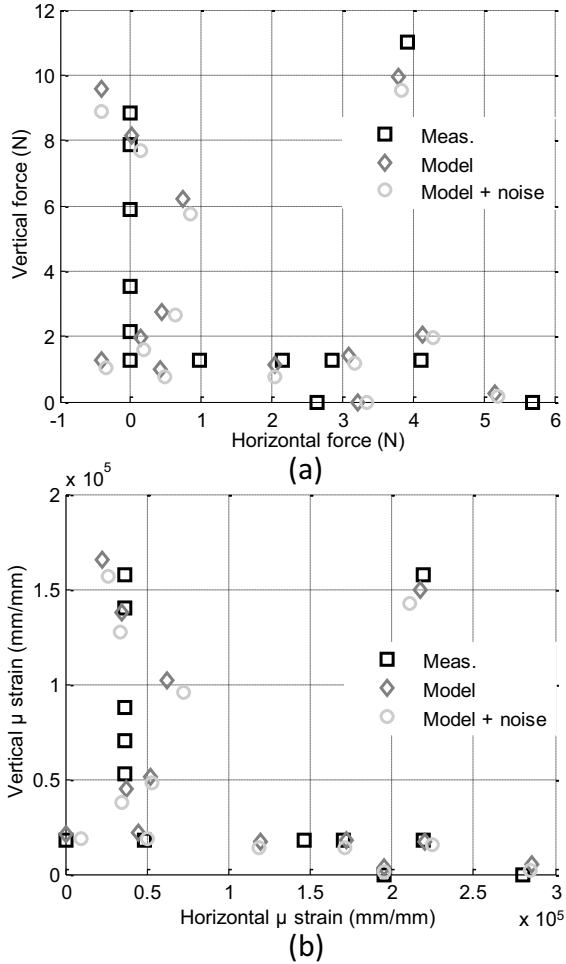


Fig. 16. 2-D diagram of applied (a) tensile forces and (b) micro-strain, on the sewn sensor. The measured values are compared to those extracted with the multi linear regression model (see Fig. 15 and equation (2) to (5)) with and without additional white gaussian noise.

$$RCS_h^e = c \cdot f + d \quad (3)$$

$$\underline{F} = \underline{L} \bullet \underline{RCS}_{coeff}^e \quad (4)$$

$$\begin{bmatrix} F_v \\ F_h \end{bmatrix} = \begin{bmatrix} L_{11} & L_{12} & L_{13} & L_{14} \\ L_{21} & L_{22} & L_{23} & L_{24} \end{bmatrix} \bullet \begin{bmatrix} a \\ b \\ c \\ d \end{bmatrix} \quad (5)$$

Let's focus on the measurement results in Fig. 9(a) and (b) obtained for several random 2-D stretching values. We applied the modeling technique described Fig. 15. We compared in Fig. 16.(a) and (b) the measured tensile forces values and micro-strains values, respectively, with the ones estimated by the model. Figure 16(a) represents the measured 2-D tensile forces map. It clearly shows the different tensile force combinations that have been measured and estimated by the introduced model. The points of the map are well spread within the detection range. The differences between the estimated and the measured values are now smaller and the maximum tensile force error value is 1 N ($\mu\epsilon = 1.87 \times 10^4$) for the vertical axis, and 0.75 N ($\mu\epsilon = 2.72 \times 10^4$) for the horizontal one. Thus, this novel technique reduces the

tensile force error by a factor of two, compared to the first extraction technique shown in Fig. 12 and 13. Concerning the strain, the error is divided by four in horizontal axis. This confirms the reliability of the extracted model. Increasing the number of the measurements to compute the regression model is a possible way to minimize the errors even more. We also tested the robustness of the model by adding artificial random noise to the RCS measurements. Figures 16(a) and (b) show what happens when tensile forces and strains are estimated, for a signal to noise ratio (SNR) of 10dB, corresponding to a noise power ten times lower than the maximum signal power. The maximum tensile force error is increased to 1.61 N ($2.2 \times 10^4 \mu\epsilon$) in the vertical axis, and 0.98 N ($2.84 \times 10^4 \mu\epsilon$) in the horizontal axis. Still, these results are well correlated with the directly measured values with the help of hanging scales and ruler.

V. DISCUSSION

The chipless sewn sensor studied in this paper, shows that it is possible to wirelessly detect a tensile force or a strain in 2-D. The measured error of the extracted model is close to 1 N. Thus, in terms of force, the sensitivity of this sewn sensor is also close to 1 N. For other applications, the weight parameter is preferred. In this case, a sensitivity of 100 g can be measured remotely. For structural health monitoring of civilian building, the value of the strain and its direction is useful. This value is usually given in micro-strain. Compared to current strain sensors, the accuracy performed by this novel design is less (commonly hundreds of micro-strains). However, the strain range from 0 up to $2.8 \times 10^5 \mu\epsilon$ can at least, provide qualitative information about deformation strength as well as about the its direction. Moreover, the relatively large theoretical read ranges enabled by the introduced processing technique, constitute significant advantages.

For a practical implementation of this technology, the expensive VNA will be replaced by a low cost dedicated FSCW radar operating in the ISM band from 2.4 GHz to 2.5 GHz as in [24], or a FMCW radar [25].

To implement a FSCW radar, a voltage controlled oscillator (VCO) is connected to a transmitting antenna through a power amplifier. For detecting the reflected power, a receiving antenna is connected to a down mixing converter for which the local oscillator (LO) input is extracted from the transmitted signal. After down mixing, the low-frequency signal is connected to a power detector. The estimated cost [24] is close to 2000 \$ for operating frequency between 5 and 10.6 GHz. Thus, it would probably be even less for operating frequencies between 2.4 GHz and 2.5 GHz. For an operating frequency within the ISM band around 2.45GHz, the federal communications commission (FCC) defines a maximum radiating power EIRP of 36 dBm if an antenna with a gain of 6 dBi is used. Let's calculate the maximum detection range using the radar equation in (6). The terms P_{tx} and P_{rx} represent the transmitted power and the received power detected by the radar, respectively. The target with a RCS denoted σ is R distant from the radar. G_{tx} and G_{rx} are the antenna gain of the transmission antenna and the receiving antenna, respectively.

TABLE I
THEORETICAL READ RANGES CALCULATED AT 2.45 GHz

Rx. antenna gain	P_{rx}^{min}	P_{tx}^{eirp}	RCS _{min}	R_{max}
Grx = 6 dBi	-74 dBm	36 dBm	-31 dBsm	7 m
Grx = 10 dBi	-74 dBm	36 dBm	-31 dBsm	8.8 m
Grx = 20 dBi	-74 dBm	36 dBm	-31 dBsm	15.6 m
Grx = 30 dBi	-74 dBm	36 dBm	-31 dBsm	27.8 m

From (6), we can obtain the equation (7) to calculate the maximum detection range for the authorized radiating power P_{tx}^{eirp} that contains the term G_{tx} . Its value is 36 dBm. We define the minimum RCS level for a reliable detection as σ_{min} . Based on the measured results for the current design, we may set this value to -31 dBsm. The power sensitivity level P_{rx}^{min} represents the threshold power detectable by the radar system. The floor noise often defines this value. For a noise floor of -80 dBm, and with a common margin of 6 dB, we obtain finally a sensitivity value of -74 dBm. For the sake of simplicity, the receiving antenna gain can be chosen to 6 dBi, as for the transmission antenna. However, it is noteworthy, that the gain of the receiving antenna does not face any power restrictions.

$$\frac{P_{rx}}{P_{tx}} = G_{tx} \cdot G_{rx} \cdot \frac{\lambda^2}{(4 \cdot \pi)^3 \cdot R^4} \cdot \sigma \quad (6)$$

$$R^{max} = \sqrt[4]{P_{tx}^{eirp} \cdot G_{rx} \cdot \frac{\lambda^2}{(4 \cdot \pi)^3 \cdot P_{rx}^{min}} \cdot \sigma_{min}} \quad (7)$$

Table I gathers calculated theoretical maximum read ranges for several receiving antenna gain values and for an operating frequency of 2.45 GHz. A detection range of 7 m can be achieved with a receiving antenna gain of 6 dBi, whereas more than 20 m is possible if using a high-gain antenna, or an additional low noise amplifier. It is to be noted that these theoretical values are obtained when the radiating power regulations defined by the FCC for the ISM band at 2.45 GHz are followed.

VI. CONCLUSION

A concept of a 2-D deformation chipless sensor sewn on stretchable fabric has been presented and validated by a measurement set-up composed of a VNA and an antenna, to implement a FSCW radar technique. It was proven that using two rectangular SRR scatterers, it is possible to separate the strain and the stress applied along two orthogonal directions. This has been made possible using a dual-polarization antenna to record the vertical, and the horizontal polarization responses generated by the chipless sensor. A new detection method for the 2-D strain extraction was experimented. We can decompose its principle into two steps:

- The first step consists in extracting a 1st order polynomial approximation of the measured RCS response in the two polarizations, from 2.4 GHz to 2.5GHz.

- The second step is to use the extracted polynomial coefficients as inputs of a multi-linear regression model to attain the estimated strain or force values.

We measured, strain range up to $1.6 \times 10^5 \mu\epsilon$ and $2.8 \times 10^5 \mu\epsilon$ in vertical and horizontal polarization, respectively. The processing of the 2-D strain can be performed based on the recorded EM response points in the ISM band at 2.45 GHz, so that a radiating power as high as 36 dBm can be emitted from the transmission antenna. As a result, a theoretical detection range of 7 m could be achieved for a receiving antenna gain of 6 dBi. Future works will focus on the practical implementation of this technology for structural health monitoring application.

ACKNOWLEDGMENT

This research has been funded by Finnish Funding Agency for Technology and Innovation, Academy of Finland and Centennial Foundation of Finnish Technology Industries. The authors are also grateful to the NSF and the NEDO.

REFERENCES

- [1] K. Finkenzerler, *RFID Handbook: Fundamentals and Applications in Contactless Smart Cards, Radio Frequency Identification and Near-field Communication*. New York, NY, USA: Wiley, 2010.
- [2] R. Bhattacharyya, C. Floerkemeier, S. Sarma, and D. Deavours, "RFID tag antenna based temperature sensing in the frequency domain," in *Proc. IEEE Int. Conf. RFID*, Apr. 2011, pp. 70–77.
- [3] S. Manzari, C. Occhiuzzi, S. Nawale, A. Catini, C. Di Natale, and G. Marrocco, "Polymer-doped UHF RFID tag for wireless-sensing of humidity," in *Proc. IEEE Int. Conf. RFID*, Apr. 2012, pp. 124–129.
- [4] C. Occhiuzzi, C. Paggi, and G. Marrocco, "Passive RFID strain-sensor based on meander-line antennas," *IEEE Trans. Antennas Propag.*, vol. 59, no. 12, pp. 4836–4840, Dec. 2011.
- [5] X. Yi, T. Wu, Y. Wang, R. T. Leon, M. M. Tentzeris, and G. Lantz, "Passive wireless smart-skin sensor using RFID-based folded patch antennas," *Int. J. Smart Nano Mater.*, vol. 2, no. 1, pp. 22–38, 2011.
- [6] L. Yang, R. Zhang, D. Staiculescu, C. P. Wong, and M. M. Tentzeris, "A novel conformal RFID-enabled module utilizing inkjet-printed antennas and carbon nanotubes for gas-detection applications," *IEEE Antennas Wireless Propag. Lett.*, vol. 8, no. 1, pp. 653–656, Jan. 2009.
- [7] C. Mandel, B. Kubina, M. Schüssler, and R. Jakoby, "Passive chipless wireless sensor for two-dimensional displacement measurement," in *Proc. 41st EuMC*, Oct. 2011, pp. 79–82.
- [8] C. Mandel, M. Schüssler, and R. Jakoby, "A wireless passive strain sensor," in *Proc. IEEE Sensors*, Oct. 2011, pp. 207–210.
- [9] S. Shrestha, M. Balachandran, M. Agarwal, V. V. Phoha, and K. Varshramyan, "A chipless RFID sensor system for cyber centric monitoring applications," *IEEE Trans. Microw. Theory Tech.*, vol. 57, no. 5, pp. 1303–1309, May 2009.
- [10] T. Thai, F. Chebila, J. Mehdi, P. Pons, H. Aubert, G. Dejean, M. Tentzeris, and R. Plana, "Design and development of a millimetre-wave novel passive ultrasensitive temperature transducer for remote sensing and identification," in *Proc. EuMC*, 2010, pp. 45–48.
- [11] A. Vena, E. Perret, S. Tedjini, D. Kaddour, A. Potie, and T. Barron, "A compact chipless RFID tag with environment sensing capability," in *IEEE MTT-S Dig.*, Jun. 2012, pp. 1–3.
- [12] P. Kalansuriya, R. Bhattacharyya, S. Sarma, and N. Karmakar, "Towards chipless RFID-based sensing for pervasive surface crack detection," in *Proc. IEEE Int. Conf. RFID Technol. Appl.*, Nov. 2012, pp. 46–51.
- [13] M. Jatlaoui, F. Chebila, P. Pons, and H. Aubert, "Pressure sensing approach based on electromagnetic transduction principle," in *Proc. Asia Pacific Microw. Conf.*, 2008, pp. 1–4.
- [14] F. Chebila, M. Jatlaoui, P. Pons, and H. Aubert, "Pressure measurement from the RADAR interrogation of passive sensors," in *Proc. IEEE Int. Symp. Antennas Propag.*, Jul. 2010, pp. 1–4.
- [15] T.-T. Thai, F. Chebila, M. Jatlaoui, P. Pons, H. Aubert, G. R. De Jean, M. M. Tentzeris, and R. Plana, "A novel passive ultrasensitive RF temperature transducer for remote sensing and identification utilizing RADAR cross sections variability," in *Proc. IEEE Antennas Propag. Symp.*, Jul. 2010, pp. 1–4.

- [16] A. Traille, S. Bouaziz, S. Pinon, P. Pons, H. Aubert, A. Boukabache, and M.-M. Tentzeris, "A wireless passive RCS-based temperature sensor using liquid metal and microfluidics technologies," in *Proc. 41st Eur. Microw. Conf.*, Oct. 2011, pp. 45–48.
- [17] C. S. Hartmann, "A global SAW ID tag with large data capacity," in *Proc. IEEE Ultrason. Symp.*, Oct. 2002, pp. 65–69.
- [18] R. Nair, E. Perret, and S. Tedjini, "Temporal multi-frequency encoding technique for chipless RFID applications," in *Proc. IEEE MTT-S*, Jun. 2012, pp. 1–3.
- [19] I. Jalaly and D. Robertson, "RF barcodes using multiple frequency bands," in *Proc. IEEE MTT-S*, Jun. 2005, pp. 139–142.
- [20] J. McVay, A. Hoorfar, and N. Engheta, "Space-filling curve RFID tags," in *Proc. IEEE Radio Wireless Symp.*, Jan. 2006, pp. 199–202.
- [21] S. Preradovic and N. C. Karmakar, "Multiresonator based chipless RFID tag and dedicated RFID reader," in *Proc. IEEE MTT-S*, May 2010, pp. 1520–1523.
- [22] A. Vena, E. Perret, and S. Tedjini, "Chipless RFID tag using hybrid coding technique," *IEEE Trans. Microw. Theory Tech.*, vol. 59, no. 12, pp. 3356–3364, Dec. 2011.
- [23] C. Mandel, B. Kubina, M. Schüssler, and R. Jakoby, "Group-delay modulation with metamaterial-inspired coding particles for passive chipless RFID," in *Proc. IEEE Int. Conf. RFID Technol. Appl.*, Nov. 2012, pp. 203–207.
- [24] S. Preradovic, N. C. Karmakar, and M. Zenere, "UWB chipless tag RFID reader design," in *Proc. IEEE Int. Conf. RFID-TA*, Jun. 2010, pp. 257–262.
- [25] H. Aubert, F. Chebila, M. Jatlaoui, T. Thai, H. Hallil, A. Traille, S. Bouaziz, A. Rifai, P. Pons, P. Menini, and M. Tentzeris, "Wireless sensing and identification of passive electromagnetic sensors based on millimetre-wave FMCW RADAR," in *Proc. IEEE Int. Conf. RFID-TA*, Nov. 2012, pp. 98–403.
- [26] A. Ramos, D. Girbau, A. Lazaro, and S. Rima, "IR-UWB radar system and tag design for time-coded chipless RFID," in *Proc. 6th EUCAP*, Mar. 2012, pp. 2491–2494.
- [27] A. Vena, E. Moradi, K. Koski, A. A. Babar, L. Sydänheimo, L. Ukkonen, and M. M. Tentzeris, "Design and realization of stretchable sewn chipless RFID tags and sensors for wearable applications," in *Proc. IEEE Int. Conf. RFID*, Apr. 2013, pp. 1–3.
- [28] Y. Kim, K. Lee, Y. Kim, and Y. Chung, "Wearable UHF RFID tag antenna design using flexible electro-thread and textile," in *Proc. IEEE Antennas Propag. Soc. Int. Symp.*, Jun. 2007, pp. 5487–5490.
- [29] G. Kim, J. Lee, K. H. Lee, Y. C. Chung, J. Yeo, B. H. Moon, J. Yang, and H. C. Kim, "Design of a UHF RFID fiber tag antenna with electric-thread using a sewing machine," in *Proc. IEEE Microw. Conf. Asia-Pacific*, Dec. 2008, pp. 1–4.
- [30] E. Moradi, T. Björminen, L. Ukkonen, and Y. Rahmat-Samii, "Characterization of embroidered dipole-type RFID tag antennas," in *Proc. IEEE Int. Conf. RFID Technol. Appl.*, Nov. 2012, pp. 248–253.
- [31] E. Koski, K. Koski, T. Björminen, A. A. Babar, L. Sydänheimo, L. Ukkonen, and Y. Rahmat-Samii, "Fabrication of embroidered UHF RFID tags," in *Proc. IEEE APSURSI*, Jul. 2012, pp. 1–2.
- [32] (2012). Shieldex Trading, Inc. *Yarns and Fillers*, Palmyra, NY, USA [Online]. Available: http://www.shieldextrading.net/yarn_and_filler.html
- [33] B. Zhang, Z. Zhou, K. Zhang, G. Yan, and Z. Xu, "Sensitive skin and the relative sensing system for real-time surface monitoring of crack in civil infrastructure," *J. Intell. Mater. Syst. Struct.*, vol. 17, no. 10, pp. 907–917, 2006.



Arnaud Vena (M'13) received the Eng. Dipl. degree in electrical engineering from Institut National Polytechnique de Grenoble (Grenoble-INP), Grenoble, France, in 2005, and the Ph.D. degree from Université de Grenoble, Grenoble, in 2012.

In 2005, he joined ACS Solution France SAS and was responsible for the development of radio frequency identification (RFID) contactless card readers. In October 2009, he started his research within Grenoble-INP, focused on the design of chipless RFID systems. He currently holds a postdoctoral

position with the Tampere University of Technology, Tampere, Finland. His current research interests include conventional and chipless RFID sensors.



Karoliina Koski received the M.Sc. degree in electrical engineering from the Tampere University of Technology, in 2012, where she is currently pursuing the Ph.D. degree the Wireless Identification and Sensing Systems Research Group.

Her current research interests include wireless radio frequency identification-enabled body-centric systems including wearable passive tag antennas.



Elham Moradi received the M.Sc. degree in signal processing and communications engineering from the Tampere University of Technology, Tampere, Finland, in 2012. She is currently pursuing the Ph.D. degree with the Wireless Identification and Sensing Systems Research Group, Department of Electronics, Tampere University of Technology.

Her current research interests include radio frequency identification system, antenna design for wireless brain machine interface system, neural prostheses antennas, and low-profile antennas.



Abdul Ali Babar received the M.Sc. and Ph.D. degrees in electrical engineering from the Tampere University of Technology, Tampere, Finland, in 2009 and 2013, respectively. He is currently a Research Scientist with the Wireless Identification and Sensing Systems Research Group, Department of Electronics and Communication Engineering, Tampere University of Technology. His current research interests include radio frequency identification (RFID) systems, sensing systems, flexible electronics, RFID readers and tag antennas, nano-technology, miniaturized antennas, radio frequency systems, and their integration with wireless systems.



Lauri Sydänheimo received the M.Sc. and Ph.D. degrees in electrical engineering from the Tampere University of Technology (TUT), Tampere, Finland. He is currently a Professor and the Head of the Department of Electronics and Communications Engineering, TUT, and is the Research Director of the Rauma Research Unit, Department of Electronics and Communications Engineering, TUT. He has authored over 170 publications in radio frequency identification (RFID) tag and reader antenna design and RFID system performance improvement. His

current research interests include wireless data communication and RFID, particularly RFID antennas and sensors.



Leena Ukkonen received the M.Sc. and Ph.D. degrees in electrical engineering in 2003 and 2006, respectively. She is currently a Professor with the Department of Electronics and Communications Engineering, Tampere University of Technology (TUT), Tampere, Finland, and is leading the Wireless Identification and Sensing Systems Research Group at the TUT Department of Electronics and Communications Engineering, Rauma Research Unit. She is an Academy of Finland Research Fellow and Adjunct Professorship with the

Aalto University School of Science and Technology, Espoo, Finland. She has authored over 130 scientific publications in radio frequency identification (RFID) antenna design and industrial RFID applications. Her current research interests include RFID antenna development for tags, readers, and RFID sensors.



Manos M. Tentzeris received the Diploma degree (*magna cum laude*) in electrical and computer engineering from the National Technical University of Athens, Athens, Greece, and the M.S. and Ph.D. degrees in electrical engineering and computer science from the University of Michigan, Ann Arbor, MI, USA, and he is currently a Professor with the School of ECE, Georgia Institute of Technology, Atlanta, GA, USA. He has published more than 480 papers in refereed journals and conference proceedings, 5 books, and 19 book chapters. He has helped

to develop academic programs in highly integrated/multilayer packaging for RF and wireless applications using ceramic and organic flexible materials, paper-based RFID's and sensors, biosensors, wearable electronics, inkjet-printed electronics, "Green" electronics and power scavenging, nanotechnology applications in RF, microwave MEM's, SOP-integrated (UWB, multiband, mmW, conformal) antennas and heads the ATHENA research group (20 researchers). He is currently the Head of the GT-ECE Electromagnetics Technical Interest Group and he has served as the Georgia Electronic Design Center Associate Director for RFID/sensors research from 2006 to 2010 and the Georgia Tech NSF-Packaging Research Center Associate Director for RF Research and the RF Alliance Leader from 2003 to 2006. He was a recipient/co-recipient of the 2012 FiDiPro Award in Finland, the iCMG Architecture Award of Excellence, the 2010 IEEE Antennas and Propagation Society Piergiorgio L. E. Uslenghi Letters Prize Paper Award, the 2011 International Workshop on Structural Health Monitoring Best Student Paper Award, the 2010 Georgia Tech Senior Faculty Outstanding Undergraduate Research Mentor Award, the 2009 IEEE Transactions on Components and Packaging Technologies Best Paper Award, the 2009 E. T. S. Walton Award

from the Irish Science Foundation, the 2007 IEEE APS Symposium Best Student Paper Award, the 2007 IEEE IMS Third Best Student Paper Award, the 2007 ISAP 2007 Poster Presentation Award, the 2006 IEEE MTT Outstanding Young Engineer Award, the 2006 Asian-Pacific Microwave Conference Award, the 2004 IEEE Transactions on Advanced Packaging Commendable Paper Award, the 2003 NASA Godfrey "Art" Anzic Collaborative Distinguished Publication Award, the 2003 IBC International Educator of the Year Award, the 2003 IEEE CPMT Outstanding Young Engineer Award, the 2002 International Conference on Microwave and Millimeter-Wave Technology Best Paper Award, Beijing, China, the 2002 Georgia Tech-ECE Outstanding Junior Faculty Award, the 2001 ACES Conference Best Paper Award, the 2000 NSF CAREER Award, and the 1997 Best Paper Award of the International Hybrid Microelectronics and Packaging Society. He was the TPC Chair for the IEEE IMS 2008 Symposium and the Chair of the 2005 IEEE CEM-TD Workshop and he is the Vice-Chair of the RF Technical Committee (TC16) of the IEEE CPMT Society. He is the Founder and Chair of the RFID Technical Committee (TC24) of the IEEE MTT Society and the Secretary/Treasurer of the IEEE C-RFID. He is an Associate Editor of the IEEE TRANSACTIONS ON MICROWAVE THEORY AND TECHNIQUES, the IEEE TRANSACTIONS ON ADVANCED PACKAGING, and the *International Journal on Antennas and Propagation*. He was a Visiting Professor with the Technical University of Munich, Munich, Germany, in 2002, a Visiting Professor with GTRI-Ireland, Athlone, Ireland, in 2009, and a Visiting Professor with LAAS-CNRS, Toulouse, France, in 2010. He has given more than 100 invited talks to various universities and companies all over the world. He is a member of URSI-Commission D, MTT-15 committee, and Technical Chamber of Greece, an associate member of EuMA, and a fellow of the Electromagnetic Academy. He is one of the IEEE MTT-S Distinguished Microwave Lecturers from 2010 to 2012.